^{26}Mg(p,n)^{26}Al and ^{23}Na(α,n)^{26}Al reactions

R. T. Skelton and R. W. Kavanagh
W. K. Kellogg Radiation Laboratory, California Institute of Technology, Pasadena, California 91125

D. G. Sargood
School of Physics, University of Melbourne, Parkville, VIC 3052, Australia
(Received 31 March 1986; revised manuscript received 9 September 1986)

Total cross sections have been measured for the ^{26}Mg(p,n)^{26}Al reaction from threshold at $E_p=4.988$ MeV to $E_p=5.820$ MeV and for the ^{23}Na(α,n)^{26}Al reaction from threshold at $E_\alpha=3.483$ MeV to $E_\alpha=4.597$ MeV, including separate measurements to the ground and first two excited states of ^{26}Al. Thermally averaged reaction rates are tabulated over the temperature range $0.1 \leq T_9 \leq 10$ for the respective inverse reactions ^{26}Al(n,p)^{26}Mg and ^{26}Al(n, α)^{23}Na, leading to the ground state of the exit-channel nuclide with the three lowest states of ^{26}Al as "targets." These rates are compared to rates calculated on a statistical model. Astrophysical implications with respect to ^{26}Al nucleosynthesis are discussed.

I. INTRODUCTION

In 1977 Lee *et al.*[1] reported large excesses in the ^{26}Mg/^{24}Mg isotopic ratio in Ca-Al rich inclusions in the Allende meteorite. The magnitudes of the excesses in several different chemical phases correlated linearly with the ^{27}Al/^{24}Mg ratio; this suggests that the ^{26}Mg resulted from *in situ* decay of ^{26}Al, implying that solid objects of macroscopic size ($\sim$1 cm) condensed on a timescale not long compared to the half-life of ^{26}Al, 7.2×10^5yr,[2] after completion of nucleosynthesis.

This discovery has generated much interest in models of ^{26}Al production sites, including supernovae,[3–6] novae,[7–9] and spallation reactions.[10] The dominant production mechanism for ^{26}Al is expected to be the ^{25}Mg(p,γ)^{26}Al reaction and the dominant destruction mechanisms the ^{26}Al(n,p)^{26}Mg or ^{26}Al(p,γ)^{27}Si reactions, depending on the site.

A particularly exciting development in the ^{26}Al problem has been the recent reports by Mahoney *et al.*[11] and Share *et al.*[12] of detection in our galaxy of the 1809-keV γ ray characteristic of ^{26}Al decay (see Fig. 1), in amounts interpreted as representing $\sim$3 solar masses of ambient ^{26}Al in the interstellar medium. Clayton[13] has reexamined the possibility that this quantity of ^{26}Al could arise from galactic supernova contributions; he finds that supernovae would need an average ^{26}Al/^{27}Al production ratio of $\sim30\times10^{-3}$, 30 times the estimate of current models, and therefore concludes that the most probable source of the observed flux is dispersed nova contributions. Giant stars may also play a significant role[14,15] in ^{26}Al production and dissemination in the galaxy.

II. EXPERIMENT

The cross sections and calculations reported here result from six separate excitation function measurements.

(1) Total neutron yield from the ^{26}Mg(p,n_{tot})^{26}Al reaction.

(2) Delayed annihilation radiation yield from the ^{26}Mg(p,n_1)^{26}Al reaction.

(3) 417-keV γ-ray yield from the ^{26}Mg(p,n_2)^{26}Al reaction.

(4) Total neutron yield from the ^{23}Na(α,n_{tot})^{26}Al reaction.

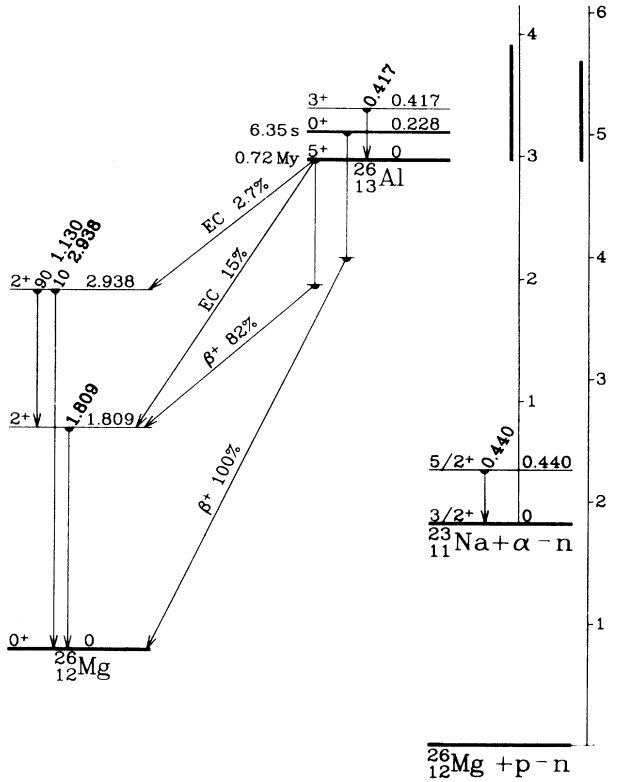

FIG. 1. Mass-26 level scheme. The vertical bars, along the center-of-mass scales on the right, show the regions investigated in the present experiments for the ^{26}Al(p,n) and ^{23}Na(α,n) reactions.

(5) Delayed positron yield from the $^{23}Na(\alpha,n_1)^{26}Al$ reaction.

(6) 417-keV γ-ray yield from the $^{23}Na(\alpha,n_2)^{26}Al$ reaction.

In the notation above the subscripts refer to the state of the exit-channel nucleus: 0 for ground state, 1 for first state, etc., with tot for total. Separate measurements to the ^{26}Al excited states are essential because production of the first-excited-state isomer ($T_{1/2}=6$ s) does not lead to long-lived ^{26}Al (see Fig. 1). Targets were in the ground state; hence a subscript 0 is understood for the incoming charged particles. Proton and alpha beams from 0.01 to 1.0 μA were supplied by an EN tandem accelerator and analyzed by a 90° magnet to a precision of ± 2 keV as determined from neutron-threshold runs with a small ^{3}He-filled counter at 0° measuring the $^7Li(p,n)$, $^{25}Mg(p,n)$, and $^{27}Al(p,n)$ yields. Energy steps of 2—3 keV were used with thin targets, described below, for all excitation function measurements, except that of the $^{23}Na(\alpha,n_1)^{26}Al$ reaction. Beam current was measured to better than $\pm 1\%$ by a conventional charge integrator; the last 77-cm length of beam pipe served as a Faraday cup. Excitation functions for the $^{26}Mg(p,n_0)^{26}Al$ and $^{23}Na(\alpha,n_0)^{26}Al$ reactions are calculated by subtracting contributions of the excited-state exit channels from the total neutron yield measurements.

Errors in target thicknesses, used in a previous report[16] of the $^{26}Mg(p,n)^{26}Al$ experiment, have been discovered, and the earlier data are superseded by the present work. The rest of this section gives details for the six different reactions.

(1) The total neutron yield from the $^{26}Mg(p,n_{tot})^{26}Al$ reaction was determined by counting neutrons in a 4π geometry. The graphite-cube neutron-detection system (GCNDS) consisted of 12 ^{3}He proportional counters symmetrically embedded in a graphite cube 1.4 m on a side. Individual discriminators for each counter were set to minimize background arising from events other than $^3He(n,p)^3H$ reactions in the counters. The entire assembly (~ 5000 kg) was mounted on rails to permit centering the detection system on the target.

The neutron detection efficiency was determined by two different techniques. Activation analysis via the $^{89}Y(p,n)^{89}Zr$ reaction gave a value of $(12.02\pm 0.08)\%$ for a neutron spectrum with $\bar{E}=450$ keV.[17] Use of a calibrated ^{252}Cf spontaneous fission source gave a value of $(12.47\pm 0.40)\%$ for its neutron spectrum ($\bar{E}=2.35$ MeV). The adopted efficiency, $(12.2\pm 0.3)\%$, is considered to be independent of energy for the neutron energies ($\lesssim 1$ MeV) encountered in these experiments, as supported by the work of Macklin.[18] Sensitivity to angular distribution and to source position were examined and found to be negligible.

The background neutron count rate for the $^{26}Mg(p,n_{tot})^{26}Al$ reaction was determined by bombarding the target below threshold and by bombarding an aluminum foil identical to the backing at various energies above and below threshold. Background contributions from contaminants in the target were found to be negligible compared to contributions from the backing. The background count rate slightly above the $^{26}Mg(p,n)^{26}Al$ threshold was 300 counts/μC, equal to the contribution from a cross section of 0.35 mb for the target used. This rate increased gradually with energy and steepened significantly above $E_p=5.5$ MeV, reaching 30 times its initial value.

^{26}Mg targets were prepared by the procedure of Takayanagi *et al.*[19] 99.7% isotopically pure ^{26}MgO was reduced with powdered Zr and evaporated onto a foil backing. ^{26}Mg target parameters are listed in Table I. Target Mg-1 was prepared with a gold layer of 275 $\mu g/cm^2$ thickness between the ^{26}Mg and the Al backing (viz., ^{26}Mg-Au-Al).

TABLE I. ^{26}Mg and ^{23}Na target parameters.

Designation	^{26}Mg or ^{23}Na thickness ($\mu g/cm^2$)	Experiment number[a]	Backing material	Notes
Mg-1	36.6 ±1.0	1,2,3	0.25 mm Al	b
Mg-2	47.2 ±2.0	1	0.25 mm Al	
Mg-3	14.3 ±0.7	2	0.25 mm Al	
Mg-4	25.2 ±1.0	2	0.25 mm Al	
Mg-5	thick	1,3		c
Mg-6	none	1,2	0.25 mm Al	d
Mg-7	8.2 ±0.6	3	0.25 mm Ta	
Mg-8	42.5 ±2.8	3	0.25 mm W	
Mg-9	none	3	0.25 mm W	d
Na-1	1.49±0.06	4,5,6	300 $\mu g/cm^2$ Au	e
Na-2	0.87±0.04	4	0.25 mm W	e
Na-3	8.9 ±1.2	5	0.25 mm W	f
Na-4	1.65±0.12	6	0.25 mm Pt	f

[a]Of six separate experiments; see text.
[b]Intermediate Au layer for Rutherford backscattering.
[c]Thick natural Mg metal.
[d]Backing material only for background determinations.
[e]Na_2WO_4 target.
[f]$Na_4P_2O_7$target.

Its ^{26}Mg thickness was determined by Rutherford backscattering of 2-MeV α particles at 160°. Backscattered α particles were counted with a Si surface-barrier detector and aperture arrangement which subtended a solid angle of 3.10×10^{-4} sr at a distance of 12.0 cm. The selected thickness of the Au layer was large enough that energy loss in it depressed the ^{27}Al backscattering edge below the entire energy range of α particles backscattered from the ^{26}Mg, but small enough that the energy range of α particles backscattered from the Au remained well separated from the energy range of those from the ^{26}Mg, as shown in Fig. 2. Straightforward analysis of the Rutherford backscattering data gave the target thickness tabulated. This target was then bombarded in the GCNDS at $E_p=5.334$ MeV and the observed neutron count rate led to a cross section of (67±3) mb at the peak of a broad maximum at this energy. The tabulated thickness of target Mg-2 was inferred from the cross section at this energy. An independent check of cross-section normalization was performed by bombarding a thick sample of 99.8% pure natural Mg metal (target Mg-5) at $E_p=5.257$ MeV, just below the ^{25}Mg(p,n)^{25}Al reaction threshold. The thick-target yield was compared to the integral over the thin-target yield to solve for the overall normalization; the cross section at $E_p=5.334$ MeV inferred by this method was (69±3) mb, in excellent agreement.

(2) Delayed annihilation radiation yield from the ^{26}Mg(p,n$_1$)^{26}Al reaction was measured with a 7.5 cm diam by 7.5 cm height NaI(Tl) crystal 2 cm from target Mg-3, which was surrounded by sufficient Al to stop all positrons except those emitted into a narrow cone up the beamline. A bombard-and-count cycle was used, with both magnetic and mechanical beam chopping, and the detector signal was not processed while the beam was on the target. Bombardment time was ~6 s, count time was ~10 s, and 20 cycles were used per energy point; the applicable formula for decay corrections is given by Bashkin *et al.*[20] A thicker target, Mg-4, was used for cross-section normalization. Its total ^{26}Mg thickness was determined from the neutron yield in the GCNDS at $E_p=5.334$ MeV. Then with a 100-cm^3 Ge(Li) detector placed 15 cm from the target, the delayed annihilation radiation was measured in a bombard-and-count cycle at the same bombarding energy. Detection efficiency for annihilation radiation was determined with a calibrated ^{22}Na source to be $(1.68\pm0.04)\times10^{-3}$ full-energy peak counts per ^{22}Na positron, corrected to $(1.62\pm0.04)\times10^{-3}$ full-energy peak counts per ^{26}Al^m positron in view of the slightly higher annihilation in flight for the more energetic positrons. The deduced ^{26}Mg(p,n$_1$)^{26}Al cross section at $E_p=5.334$ MeV is (62±3) mb, which was used to normalize the relative data from target Mg-3.

(3) The 417-keV γ-ray yield from the ^{26}Mg(p,n$_2$)^{26}Al reaction was measured using a thin target (Mg-7) with a 60-cm^3 Ge(Li) detector (5.0 cm diam) placed at a distance of 6 cm and an angle of 125°, a zero of $P_2(\cos\theta)$. The data obtained thus represent total cross sections to the extent that terms in $P_4(\cos\theta)$ can be neglected. (The maximum possible error from this neglect is 1.2%, which would occur for the 3^+ level fully aligned in the $m=\pm2$ substate, and this is further reduced to 0.9% in the given geometry.) Targets Mg-8 and Mg-9 were used for normalization. The ^{26}Mg thickness of Mg-8 was determined by total neutron yield in the GCNDS at $E_p=5.334$ MeV, with Mg-9 establishing that the background from the W was 22% of the total neutron counts. Mg-8 was then bombarded at $E_p=5.545$ MeV, and the 417-keV γ-ray yield was measured with the 100-cm^3 Ge(Li) detector (5.0 cm diam) at a distance of 16 cm and an angle of 125°. The efficiency for this Ge(Li) system was measured by substituting a calibrated ^{152}Eu source for the target; the full-energy peak efficiency at $E_\gamma=417$ keV was (0.104±0.002)%, and the ^{26}Mg(p,n$_2$)^{26}Al cross section at $E_p=5.545$ MeV is (245±15) mb. An independent check of normalization for the ^{26}Mg(p,n$_2$)^{26}Al reaction was also made via the 417-keV γ-ray yield from a thick target of natural Mg [analogous to that described above for the ^{26}Mg(p,n$_{tot}$)^{26}Al reaction]. Target Mg-5 was bombarded at $E_p=5.800$ MeV, and the cross section inferred from the data is (238±25) mb at $E_p=5.545$ MeV, in excellent agreement.

(4) The total neutron yield from the ^{23}Na(α,n$_{tot}$)^{26}Al reaction was determined with target Na-2 in the GCNDS (see Table I). Target-thickness measurement was again a critical experimental detail, and a special thin target (Na-1) of Na_2WO_4 was prepared on 300-μg/cm^2 Au to facilitate backscattering measurement. The transmitted beam was stopped in high-purity Cu for the measurement of total neutron yield and in graphite for Rutherford backscattering. The backscattering geometry was similar to that used for target Mg-1. Figure 3 shows the backscattering spectrum obtained; analysis of this spectrum led to the tabulated thickness and a cross section of (43±2) mb at $E_\alpha=4.147$ MeV. Below the threshold for the ^{23}Na(α,n)^{26}Al reaction, resonances in the (α,n) excitation functions of two common contaminants, ^{18}O and ^{13}C,

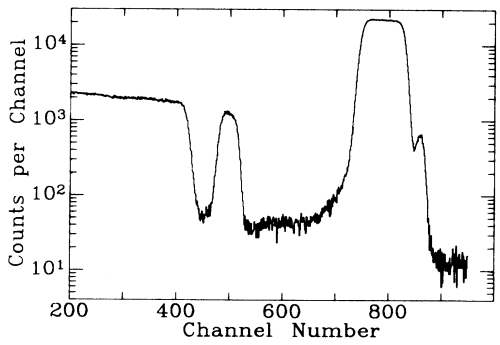

FIG. 2. The Rutherford backscattering spectrum of 2-MeV α particles, at $\theta_{lab}=160°$, from the ^{26}Mg-Au-Al sandwich target described in text. The step near channel 420 is from the thick Al backing, the peak around channel 500 from the Mg surface layer, and the peak near channel 800 from the intermediate Au layer. The small peak near channel 870 is attributed to scattering from surface Au, probably due to pinholes in the Mg layer. The Au layer served to shift the Al edge downward in energy, leaving the Mg peak clearly resolved.

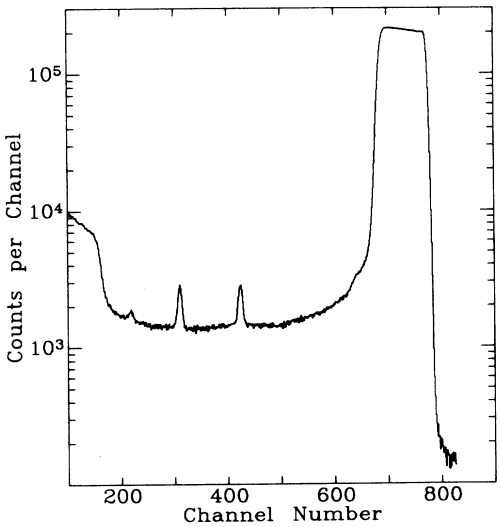

FIG. 3. The backscattering spectrum from the Na_2WO_4 target on a thin Au foil, showing peaks near channels 220, 310, 430, and 700 due to surface carbon contamination, O, Na, and W + Au, respectively. The edge near channel 160 is due to scattering from the graphite beam stop.

were examined, and the amount of each contaminant was determined; within uncertainties, the contributions from these accounted for all of the yield observed below the threshold of the $^{23}Na(\alpha,n)^{26}Al$ reaction. Excitation functions for (α,n) reactions on these two contaminants were used to perform the background subtraction. Background at the largest resonances was ~ 600 counts/μC, equal to the contribution from 2.0 mb in the $^{23}Na(\alpha,n)^{26}Al$ cross section from target Na-2.

(5) Delayed positron yield from the $^{23}Na(\alpha,n_1)^{26}Al$ reaction was measured by a conventional plastic scintillator and photomultiplier tube. Preliminary investigation showed that the yield from this reaction was substantially lower than the others examined. To maximize detection efficiency, the target, Na-3, was mounted at the end of a thin-wall (0.25 mm) stainless steel cell which was inserted into a well (1.7 cm diam, 2.5 cm depth) in the plastic scintillator; the scintillator size (5 cm diam, 5 cm height) was optimized for the $^{26}Al^m$ positrons. A pulse-height threshold corresponding to ~ 1 MeV was selected as a compromise between background rejection and detection efficiency. A bombard-and-count cycle similar to that for the $^{26}Mg(p,n_1)^{26}Al$ measurement was used. The scintillator/photomultiplier tube assembly was shielded with ~ 2 cm of Pb and placed in the center of the GCNDS, so that relative data for the excitation functions for both $^{23}Na(\alpha,n_1)^{26}Al$ and $^{23}Na(\alpha,n_{tot})^{26}Al$, as the raw data appeared from this semithick target, were simultaneously measured. The $^{23}Na(\alpha,n_{tot})^{26}Al$ excitation function previously measured from the thin target was analyzed to determine the form various features would present if the target layer were thick enough to degrade energy resolution significantly, but the total amount of ^{23}Na kept fixed. This analysis was done for energy thicknesses ranging from 20 to 150 keV. The shape for a 60-keV target thickness corresponded most closely to that observed from Na-3. The ratio of total neutron yields was then used to infer the ^{23}Na thickness of Na-3; this value, 8.9 $\mu g/cm^2$, corresponds to 25.7 $\mu g/cm^2$ of $Na_4P_2O_7$ and an energy thickness of 19 keV. The apparent discrepancy in energy thickness (19 vs 60 keV) is ascribed to intermixing of the $Na_4P_2O_7$ and the W backing. Slight intermixing of target material into the backing had been observed on the thin targets under much lower beam currents. (The target materials most resistant to mixing with the backing under bombardment were $Na_4P_2O_7$ and Na_2WO_4; NaCl and NaOH, in particular, were unsatisfactory.)

Thin-target analysis has been applied to the $^{23}Na(\alpha,n_1)^{26}Al$ data for several reasons. First, uncertainties arising from the actual ^{23}Na distribution within the target layer are such that an attempt at a more sophisticated analysis would be more a mathematical exercise than a legitimate refinement of the data. Second, the quantity of most interest is the thermally averaged reaction-rate factor. The contributions to this factor from a given resonance depends only on the integral $\int \sigma(E)dE$, a quantity which is unchanged to first order if thin-target analysis is applied to a semithick target. Third, the cross section values are small enough that subtracting the partially integrated $^{23}Na(\alpha,n_1)^{26}Al$ excitation function from the well-resolved $^{23}Na(\alpha,n_{tot})^{26}Al$ excitation function hardly affects the latter. It is emphasized, however, that the smooth shape results from experimental limitations.

With target thickness determined, normalization was accomplished by bombarding Na-3 at $E_\alpha = 4.157$ MeV. The procedure was similar to that used with Mg-4 in the $^{26}Mg(p,n_1)^{26}Al$ reaction, but with the 100-cm^3 Ge(Li) detector ~ 7 cm from the target to compensate for the lower yield. The annihilation radiation detection efficiency was $(6.2\pm0.2)\times10^{-3}$ counts in the full-energy peak per positron, leading to a cross section of (1.72 ± 0.20) mb at $E_\alpha = 4.157$ MeV.

(6) The 417-keV γ-ray yield from the $^{23}Na(\alpha,n_2)^{26}Al$ reaction was measured by a procedure similar to that used for the $^{26}Mg(p,n_2)^{26}Al$ reaction. The thickness of target Na-4 was determined from total neutron yield at $E_\alpha = 4.147$ MeV compared to Na-1. Normalization was accomplished with the 100-cm^3 Ge(Li) detector 7 cm from the target, with a detection efficiency of $(1.04\pm0.03)\%$ at $E_\gamma = 417$ keV; this led to an absolute cross section for the $^{23}Na(\alpha,n_2)^{26}Al$ reaction of (16.1 ± 1.0) mb at $E_\alpha = 4.509$ MeV.

III. RESULTS

Figure 4 shows the results of the analysis of the $^{26}Mg(p,n_i)^{26}Al$ data. The estimated precision for the total neutron data is $\pm(5\%+0.1$ mb); the 5% arises primarily from uncertainties in the overall normalization, while the 0.1 mb arises from uncertainties in background subtraction. The estimated precision of the data for the first excited state is $\pm(6\%+30\ \mu b)$; for the second excited state, it is $\pm(8\%+0.3$ mb). The excitation function for production of the ground state of ^{26}Al was determined by subtracting the excitation functions for the other two states

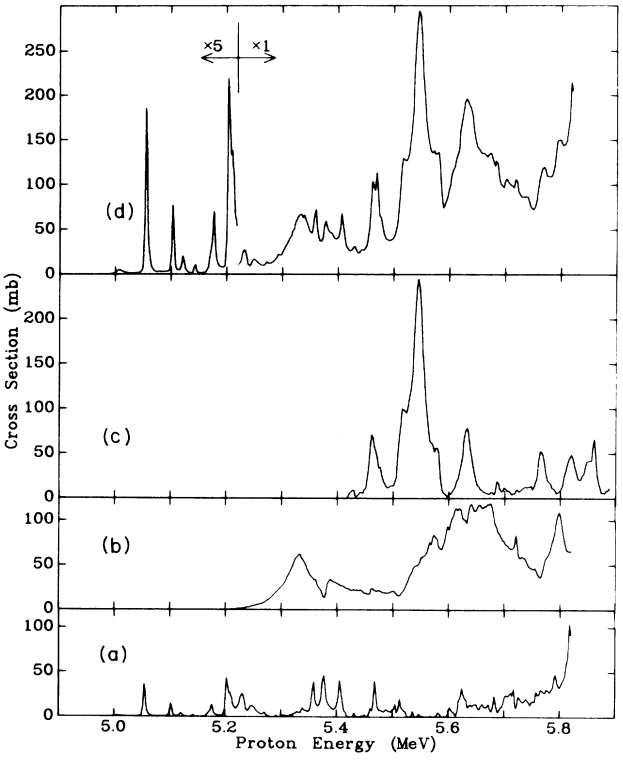

FIG. 4. Excitation functions for (a) ^{26}Mg(p,n$_0$)^{26}Al, (b) ^{26}Mg(p,n$_1$)^{26}Al, (c) ^{26}Mg(p,n$_2$)^{26}Al, and (d) the total neutron yield.

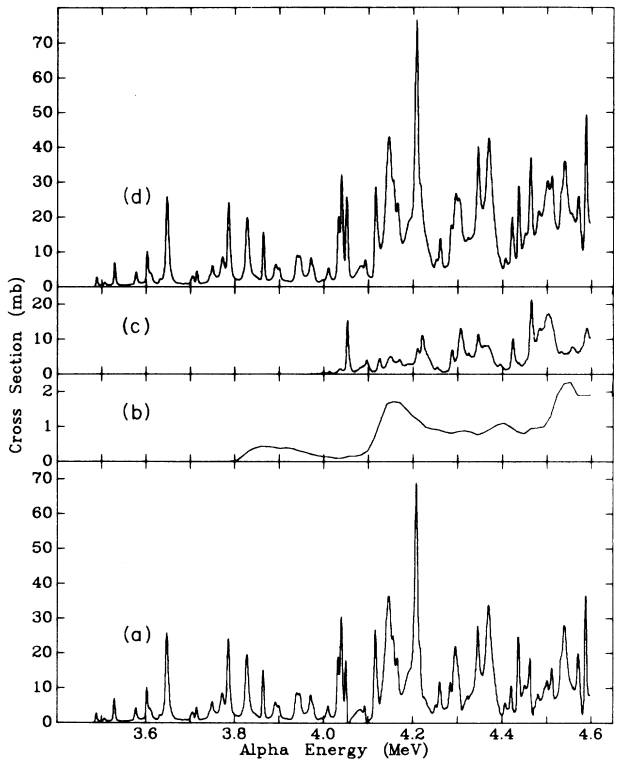

FIG. 5. Excitation functions for (a) ^{26}Mg(α,n$_0$)^{26}Al, (b) ^{26}Mg(α,n$_1$)^{26}Al, (c) ^{26}Mg(α,n$_2$)^{26}Al, and (d) the total neutron yield. In (b), note the tenfold lower ordinate and the much lower energy resolution from the thicker target used to compensate for the low cross section.

from the total, and it is therefore subject to greater uncertainties, given by the quadrature sum of those from the three independent measurements.

Figure 5 shows the results from the ^{23}Na(α,n$_i$)^{26}Al data. The estimated precision is similarly $\pm(5\%+0.3$ mb) for the total-neutron data, $\pm(15\%+5$ μb) for the first-excited-state data, and $\pm(8\%+0.1$ mb) for the second-excited-state data. The excitation function to the ground state was determined again by subtraction, and the above comment regarding ^{26}Mg(p,n$_0$)^{26}Al again applies.

Although previous experiments have been done on the ^{26}Mg(p,n)^{26}Al and ^{23}Na(α,n)^{26}Al reactions,[21–26] the present experiment is the first of sufficient resolution to permit extraction of the excitation functions leading

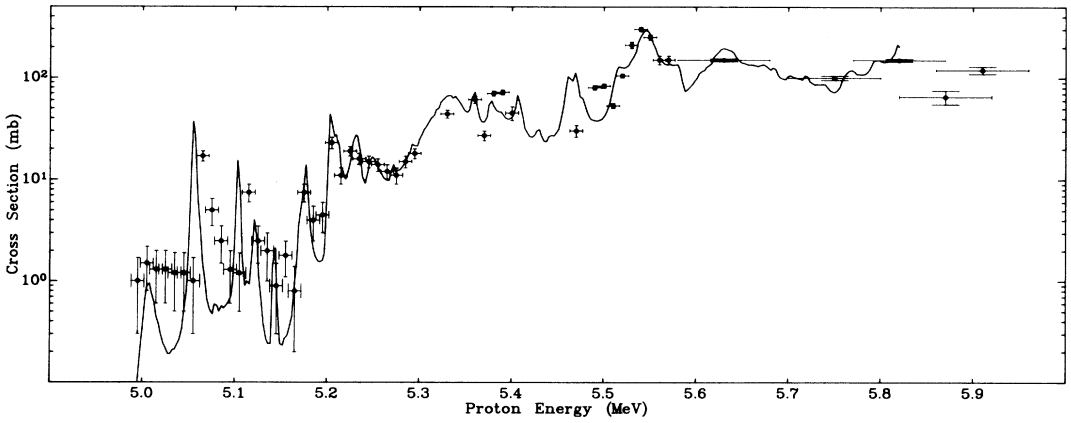

FIG. 6. Comparison of data from the present experiment [solid line, same as Fig. 4(d)] with the data of Norman *et al.* (circles with error bars; Ref. 26) for the total neutron yield in the ^{26}Mg(p,n)^{26}Al reaction.

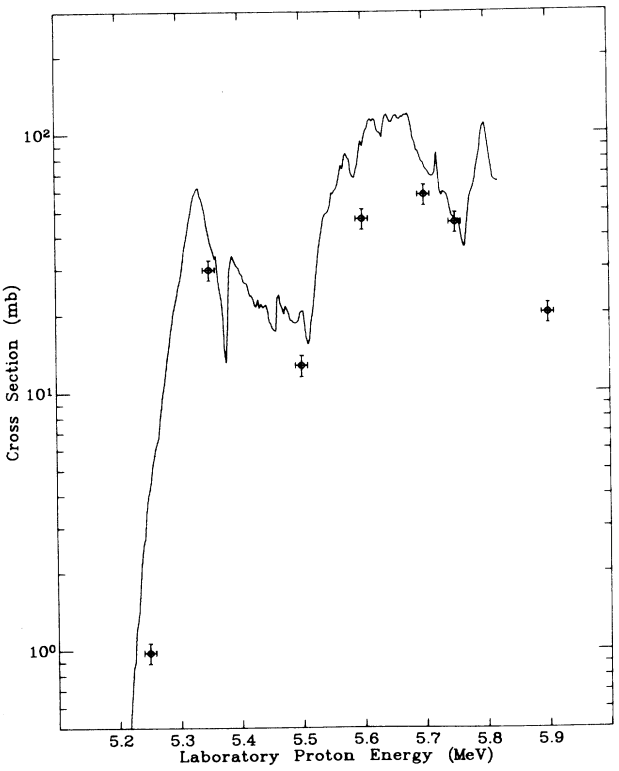

FIG. 7. Comparison of data from the present experiment [solid line, same as Fig. 4(c)] with the data of King and Cheng (circles with error bars; Ref. 23) for the yield to the first excited state in the ^{26}Mg(p,n$_1$)^{26}Al reaction.

directly to the ground state of ^{26}Al. Agreement with previous experiment is generally good. Figure 6 compares the excitation function for ^{26}Mg(p,n$_{tot}$)^{26}Al to those of Norman *et al.*,[26] the latter having been done with a thick target. Substantial disagreement occurs at isolated points, particularly in valleys beyond large resonances, where the thick-target technique is especially difficult. The most salient discrepancies are in the ^{26}Mg(p,n$_1$)^{26}Al and ^{23}Na(α,n$_1$)^{26}Al excitation functions, where the present results are higher by as much as a factor of 2 than the previous.[23,27] Figure 7 compares the present results for ^{26}Mg(p,n$_1$)^{26}Al to those of King and Cheng.[23] A complete comparison to all previous results is given in the thesis of one of the present authors (R.T.S.).[28]

IV. ANALYSIS

The principle of detailed balance (see Fowler *et al.*[29] for the applicable formula) was used to calculate the excitation functions for the ^{26}Al(n$_i$,p$_0$)^{26}Mg and ^{26}Al(n$_i$,α_0)^{23}Na reactions, where the subscript 0 indicates the ground state of ^{26}Mg or ^{23}Na, and the subscript i takes the values 0, 1, and 2. The results are displayed in Figs. 8 and 9; calculated results of the Hauser-Feshbach optical model[30] are included for comparison.

The theoretical model considerably overestimates the ^{26}Al(n$_0$,p$_0$)^{26}Mg cross section and generally underestimates that of the ^{26}Al(n$_1$,p$_0$)^{26}Mg reaction. All cross sections seem to be overestimated at low energies. While the energy denominator in the inversion formula can magnify any nonzero cross section just above the (p,n) thresholds,

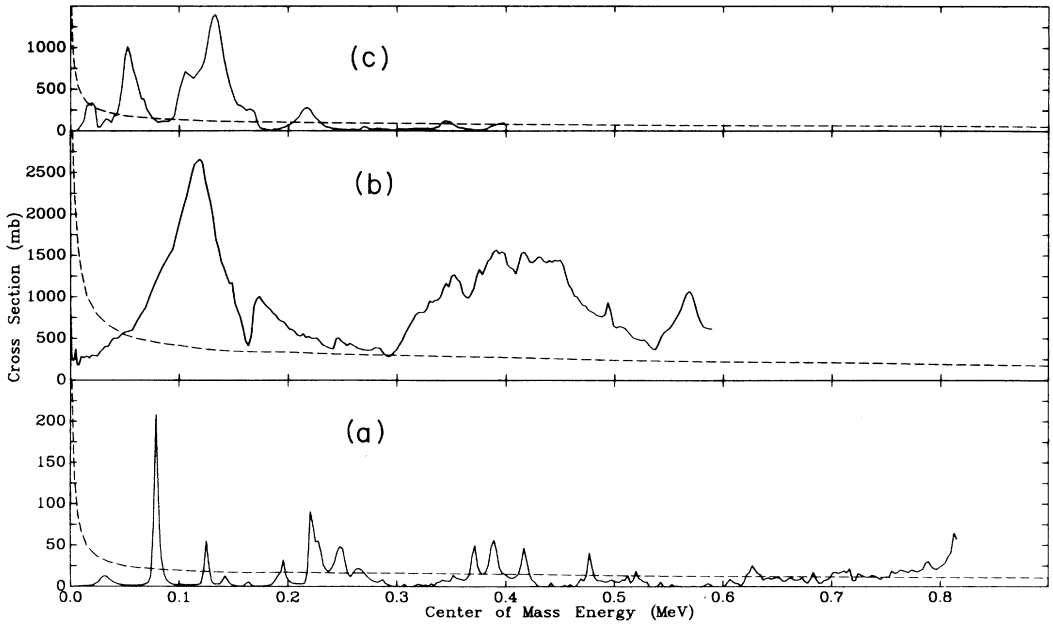

FIG. 8. Experimental excitation functions for (a) ^{26}Al(n$_0$,p)^{26}Mg, (b) ^{26}Al(n$_1$,p)^{26}Mg, and (c) ^{26}Al(n$_2$,p)^{26}Mg. These were determined by detailed balance from the data of Figs. 4(a), 4(b), and 4(c), respectively. The dashed curves show the results of the Hauser-Feshbach calculations.

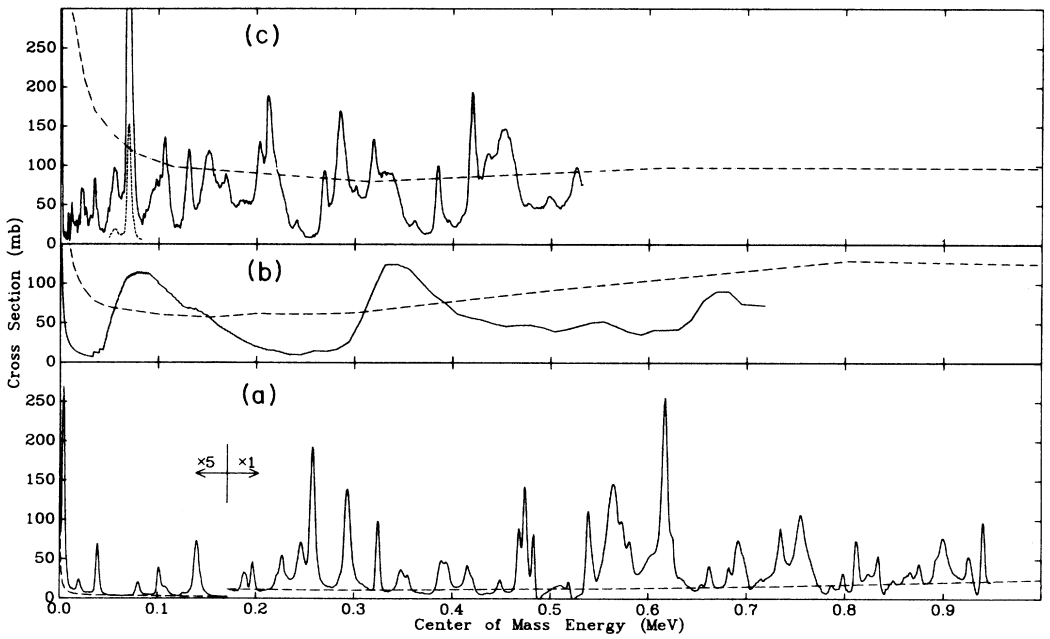

FIG. 9. Experimental excitation functions for (a) ^{26}Al(n_0,α)^{23}Na, (b) ^{26}Al(n_1,α)^{26}Na, and (c) ^{26}Al(n_2,α)^{23}Na, determined by detailed balance from the data of Figs. 4(a), 4(b), and 4(c), respectively. The dashed curves show the results of the Hauser-Feshbach calculations. The breaks in slope in the latter curves are artifacts due to the coarse energy grid used in the calculations.

for energies in the ^{26}Al+n system above 5 keV the sensitivity of the measurements was sufficient to exclude the theoretical values shown in Fig. 8.

For the ^{26}Al(n_i,α_0)^{23}Na reactions the theory again overestimates the cross section at low energies for the two excited states; for the ground state the theory underestimates the cross section at nearly all energies.

Tables II and III show the reaction rate factors $N_A\langle\sigma v\rangle$ for the ^{26}Al(n_i,p_0)^{26}Mg and ^{26}Al(n_i,α_0)^{23}Na reactions. Here, N_A is Avogadro's number, and the angular brackets refer to averaging cross section times velocity over a Boltzmann distribution. In calculating these averages, the integration was carried out numerically from $E_{\text{c.m.}}=0$ to the highest energy for which experimental data was taken. An asymptotic contribution was then added on, calculated by assuming optical-model values[30] of the cross section for energies above the highest measured. Percentage contributions from the asymptotic term are given in parentheses when they become significant in these tables.

When a cross section is inverted, a denominator factor of $E-E_{\text{thr}}$ can result in arbitrarily large values of the inverted cross section immediately above threshold. However, a factor of $E_{\text{c.m.}}$ in the formula for thermal averaging limits the contributions from small resonances just above threshold. Single unobserved resonances near the respective thresholds could add to the tabulated values for the ^{26}Al(n_i,p_0)^{26}Mg reaction rates (Table II) the amounts $N_A\langle\sigma v\rangle=4.7\times10^4T_9^{-3/2}$, $1.6\times10^4T_9^{-3/2}$, and $1.6\times10^5T_9^{-3/2}$ for $i=0$, 1, and 2, respectively. (T_9 is the temperature in 10^9 K.) For the ^{26}Al(n_i,α_0)^{23}Na reaction rates (Table III) the corresponding coefficients of $T_9^{-3/2}$

TABLE II. ^{26}Al(n,p)^{26}Mg reaction rates.[a] $N_A\langle\sigma v\rangle$ in $\text{cm}^3\,\text{mol}^{-1}\,\text{s}^{-1}$. Numbers in square brackets denote powers of ten, i.e., $[+5]=\times10^5$.

T_9	^{26}Al(n_0,p_0)^{26}Mg	^{26}Al(n_1,p_0)^{26}Mg	^{26}Al(n_2,p_0)^{26}Mg
0.10	2.32[+5]	2.64[+07]	1.25[+07]
0.15	4.95[+5]	4.10[+07]	2.22[+07]
0.20	8.30[+5]	6.07[+07]	3.21[+07]
0.30	1.51[+6]	1.10[+08]	5.03[+07]
0.40	2.05[+6]	1.57[+08]	6.53[+07]
0.50	2.46[+6]	1.94[+08]	7.60[+07]
0.60	2.79[+6]	2.22[+08]	8.28[+07]
0.70	3.07[+6]	2.44[+08]	8.65[+07]
0.80	3.31[+6]	2.60[+08]	8.88[+07] (1)
0.90	3.53[+6]	2.74[+08]	8.81[+07] (1)
1.00	3.73[+6]	2.85[+08]	8.80[+07] (2)
1.50	4.42[+6] (1)	3.21[+08] (1)	8.02[+07] (6)
2.00	4.93[+6] (5)	3.37[+08] (4)	7.22[+07] (13)
2.50	5.38[+6] (10)	3.35[+08] (6)	6.60[+07] (20)
3.00	5.73[+6] (16)	3.33[+08] (9)	6.15[+07] (27)
3.50	5.99[+6] (21)	3.22[+08] (12)	5.81[+07] (34)
4.00	6.38[+6] (28)	3.11[+08] (14)	5.57[+07] (40)
4.50	6.57[+6] (33)	2.99[+08] (18)	5.40[+07] (45)
5.00	6.75[+6] (37)	2.88[+08] (20)	5.19[+07] (50)
6.00	6.88[+6] (45)	2.67[+08] (25)	4.92[+07] (57)
7.00	7.02[+6] (52)	2.46[+08] (29)	4.70[+07] (63)
8.00	7.22[+6] (57)	2.28[+08] (32)	4.55[+07] (67)
9.00	7.31[+6] (61)	2.12[+08] (36)	4.36[+07] (71)
10.00	7.14[+6] (65)	1.97[+08] (39)	4.16[+07] (74)

[a]In the latter parts of this table and Table III, the numbers in parentheses are the percentage contributions to the reaction rates calculated from the statistical model for energies above the measured range.

TABLE III. $^{26}Al(n,\alpha)^{23}Na$ reaction rates. $N_A\langle\sigma v\rangle$ in $cm^3\,mol^{-1}\,s^{-1}$.

T_9	$^{26}Al(n_0,\alpha_0)^{23}Na$	$^{26}Al(n_1,\alpha_0)^{23}Na$	$^{26}Al(n_2,\alpha_0)^{23}Na$
0.10	0.2077[+8]	0.2366[+07]	0.4104[+07]
0.15	0.1695[+8]	0.2944[+07]	0.5418[+07]
0.20	0.1503[+8]	0.4250[+07]	0.7393[+07]
0.30	0.1343[+8]	0.7398[+07]	0.1128[+08]
0.40	0.1307[+8]	0.1000[+08]	0.1420[+08]
0.50	0.1313[+8]	0.1183[+08]	0.1631[+08]
0.60	0.1333[+8]	0.1309[+08]	0.1792[+08]
0.70	0.1356[+8]	0.1403[+08]	0.1921[+08]
0.80	0.1378[+8]	0.1480[+08]	0.2029[+08]
0.90	0.1399[+8]	0.1548[+08]	0.2122[+08]
1.00	0.1420[+8]	0.1613[+08]	0.2205[+08] (1)
1.50	0.1526[+8]	0.1924[+08] (3)	0.2518[+08] (5)
2.00	0.1632[+8] (1)	0.2226[+08] (9)	0.2724[+08] (12)
2.50	0.1720[+8] (2)	0.2511[+08] (17)	0.2872[+08] (20)
3.00	0.1784[+8] (4)	0.2776[+08] (25)	0.2988[+08] (28)
3.50	0.1829[+8] (7)	0.3020[+08] (33)	0.3087[+08] (35)
4.00	0.1860[+8] (10)	0.3245[+08] (40)	0.3177[+08] (41)
4.50	0.1885[+8] (13)	0.3451[+08] (46)	0.3262[+08] (47)
5.00	0.1907[+8] (17)	0.3639[+08] (52)	0.3342[+08] (52)
6.00	0.1955[+8] (25)	0.3961[+08] (60)	0.3491[+08] (61)
7.00	0.2013[+8] (33)	0.4220[+08] (67)	0.3624[+08] (67)
8.00	0.2084[+8] (41)	0.4421[+08] (71)	0.3740[+08] (72)
9.00	0.2162[+8] (48)	0.4572[+08] (75)	0.3836[+08] (76)
10.00	0.2244[+8] (54)	0.4678[+08] (78)	0.3914[+08] (79)

are 1.1×10^5, 3.0×10^4, and 6.1×10^4, respectively.

Figures 10 and 11 show the ratios of the reaction rates calculated from the experimental data of Figs. 8 and 9 to the corresponding reaction rates calculated using the statistical model. The ratios are not plotted for values of T_9 when the contribution from the asymptotic term exceeds

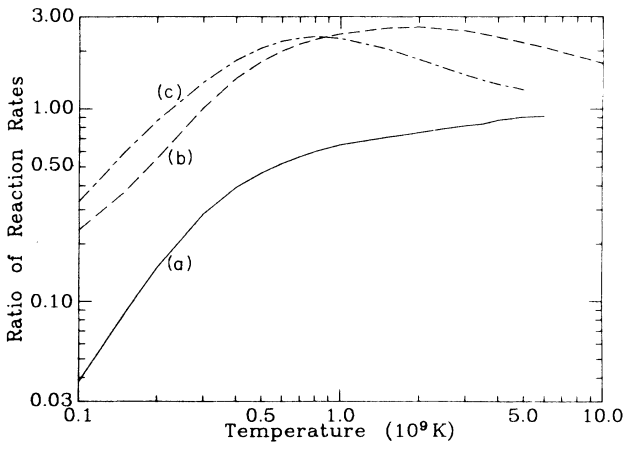

FIG. 10. Ratios of reaction rates determined from the present data to the reaction rates determined from Hauser-Feshbach cross sections, as functions of temperature, for (a) $^{26}Al(n_0,p)^{26}Mg$, (b) $^{26}Al(n_1,p)^{26}Mg$, and (c) $^{26}Al(n_2,p)^{26}Mg$. In each case, the reactions are to the *ground* state of ^{26}Mg.

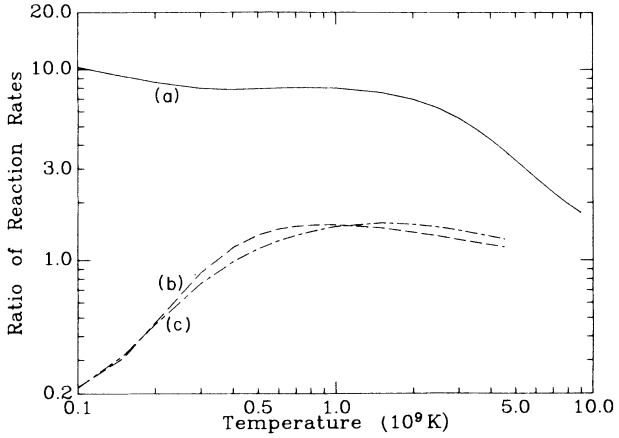

FIG. 11. Ratios of reaction rates as in Fig. 10, but for (a) $^{26}Al(n_0,\alpha)^{23}Na$, (b) $^{26}Al(n_1,\alpha)^{23}Na$, and (c) $^{26}Al(n_2,\alpha)^{23}Na$.

that from the actual experimental data; this occurs around $T_9=5$.

While good energy resolution is not necessarily essential when the end product will be thermally averaged reaction rates, its desirability is illustrated by the fractional contributions to the $^{26}Al(n_0,p_0)^{26}Mg$ reaction rate factors from the two lowest resonances. At $T_9=0.1$ the resonance at 32 keV in Fig. 8(a) contributes approximately 60% of the integral; at $T_9=0.3$ the resonance at 79 keV contributes a similar percentage.

V. DISCUSSION

Figure 12 shows several relevant reaction-rate factors calculated from the formulae of Caughlan *et al.*[31] Here the reactions $^{26}Al(n_0,p_{tot})^{26}Mg$ and $^{26}Al(n_0,\alpha_{tot})^{23}Na$ refer to *all* states of the product, ground and excited. It is noteworthy that for $T_9<2$ the experimentally determined $^{26}Al(n_0,\alpha_0)^{23}Na$ rate is significantly greater than the theoretically estimated rate for the $^{26}Al(n_0,\alpha_{tot})^{23}Na$ reaction. In fact, this experimental $^{26}Al(n_0,\alpha_0)^{23}Na$ reaction rate is a large fraction (40–65%) of the theoretically estimated $^{26}Al(n_0,p_{tot})^{26}Mg$ rate, the supposed principal destruction mechanism. If higher excited states of ^{23}Na contribute appreciably, it seems possible that $^{26}Al(n,\alpha)^{23}Na$ is, in fact, the principal destruction mechanism. In any case, the $^{26}Al(n,\alpha)^{23}Na$ reaction clearly contributes significantly to the destruction of ^{26}Al in a neutron-rich environment.

The $^{26}Al(n_0,\alpha_0)^{23}Na$ reaction rates calculated from the data of the present experiment reinforce Clayton's statement[13] that supernovae have little chance of contributing the quantity of ^{26}Al, live and fossil, which has been observed. His suggestion that contributions from novae dominate is correspondingly strengthened. (See Woosley and Weaver[8] for an example of the sensitivity of predicted

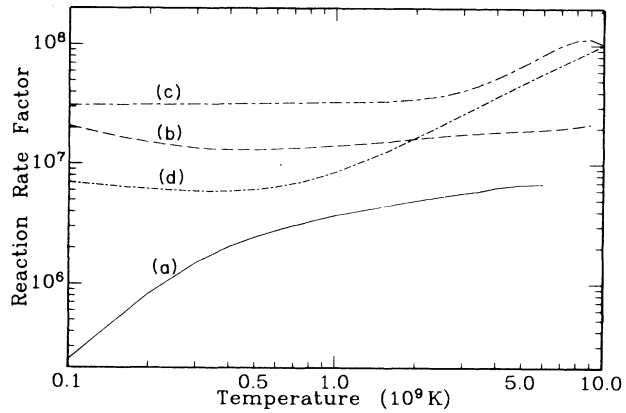

FIG. 12. The experimental reaction rates vs temperature, curves (a) and (b), from the present data for ^{26}Al(n_0,p_0)^{26}Mg and ^{26}Al(n_0,α_0)^{23}Na, respectively, and the theoretical rates, curves (c) and (d), taken from the tabulations of Caughlan *et al.* (Ref. 31), for ^{26}Al(n_0,p_{tot})^{26}Mg and ^{26}Al(n_0,α_{tot})^{23}Na, respectively. The values represented by (c) are expected to be dominated by reactions to excited states of ^{26}Mg, and are therefore much higher than (a), as is evidently true. It is, however, surprising that (b) is higher than (d): the theory apparently significantly underestimates the reaction rate for ^{26}Al(n_0,α_0)^{23}Na.

net ^{26}Al production to the neutron-induced destruction rate in supernovae.) More recent calculations[32] suggest massive mass-losing stars as promising candidates for some, or with extreme assumptions possibly all, of the observed galactic ^{26}Al. In such stars, ^{26}Al is produced during hydrogen burning by ^{25}Mg(p,γ) and destroyed by ^{26}Al(p,γ). Further destruction occurs during helium burning through the (n,p) and (n,α) reactions.

Further measurements of reactions involving ^{26}Al are clearly warranted to clarify the production and destruction mechanisms and sites. Some investigations have been made, including those by Champagne *et al.*[33] and Schmalbrock *et al.*[34] into the possibility that ^{26}Al production and/or destruction may be enhanced by low-energy resonances in the ^{25}Mg(p,γ)^{26}Al and ^{26}Al(p,γ) reactions, the study by Buchmann *et al.*[35] of the ^{26}Al(p,γ)^{27}Si reaction, and the direct measurements of the ^{26}Al(n,p)^{26}Mg reaction by Trautvetter *et al.*,[36] who obtained results in good agreement with the present work for ^{26}Al(n_0,p_0)^{26}Mg.

It should be emphasized that nucleosynthesis models often require reaction rates involving excited states in both entrance and exit channels.[37] Laboratory measurement of cross sections between the short-lived excited states for ^{23}Na, ^{26}Mg, and ^{26}Al would appear impossible, and we are obliged to depend on the theoretical calculations, tested against similar measurable cases.

ACKNOWLEDGMENTS

Useful discussions with W. A. Fowler are gratefully acknowledged. This work was supported in part by the National Science Foundation Under Grant Nos. PHY85-05682 and PHY82-15500.

[1]T. Lee, D. A. Papanastassiou, and G. J. Wasserburg, Astrophys. J. Lett. **211**, L107 (1977).
[2]J. H. Thomas, R. L. Rau, R. T. Skelton, and R. W. Kavanagh, Phys. Rev. C **30**, 385 (1984).
[3]W. D. Arnett and J. P. Wefel, Astrophys. J. Lett. **224**, L139 (1978).
[4]J. W. Truran and A. G. W. Cameron, Astrophys. J **219**, 226 (1978).
[5]S. E. Woosley, T. S. Axelrod, and T. A. Weaver, Comments Nucl. Part. Phys. **9**, 185 (1981).
[6]D. D. Clayton, in *Essays in Nuclear Astrophysics,* edited by C. A. Barnes, D. D. Clayton, and D. N. Schramm (Cambridge University Press, Cambridge, 1982), p. 401.
[7]M. Arnould, H. Nørgaard, F.-K. Thielemann, and W. Hillebrandt, Astrophys. J. **237**, 931 (1980).
[8]S. E. Woosley and T. A. Weaver, Astrophys. J. **238**, 1017 (1980).
[9]W. Hillebrandt and F.-K. Thielemann, Astrophys. J. **255**, 617 (1982).
[10]Typhoon Lee, Astrophys. J. **224**, 217 (1978).
[11]W. A. Mahoney, J. C. Ling, W. A. Wheaton, and A. S. Jacobson, Astrophys. J. **286**, 578 (1984).
[12]G. H. Share, R. L. Kinzer, J. D. Kurfess, D. J. Forrest, E. L. Chupp, and E. Rigger, Astrophys. J. **292**, L61 (1985).
[13]D. D. Clayton, Astrophys. J. **280**, 144 (1984).
[14]H. Nørgaard, Astrophys. J. **236**, 895 (1980).
[15]D. S. P. Dearborn and J. B. Blake, Astrophys. J. Lett. **288**, L21 (1985).
[16]R. T. Skelton, R. W. Kavanagh, and D. G. Sargood, Astrophys. J. **271**, 404 (1983); **308**, 485(E) (1986).
[17]R. T. Skelton and R. W. Kavanagh, Nucl. Phys. **A414**, 141 (1984).
[18]R. L. Macklin, Nucl. Instrum. **1**, 335 (1957).
[19]S. Takayanagi, M. Katsuta, K. Katori, and R. Chiba, Nucl. Instrum. Methods **45**, 345 (1966).
[20]S. Bashkin, R. W. Kavanagh, and P. D. Parker, Phys. Rev. Lett. **3**, 518 (1959).
[21]C. Wong, J. D. Anderson, J. W. McClure, and B. Pohl, Phys. Rev. **156**, 1266 (1967).
[22]M. Furukawa, K. Shizuri, K. Komura, K. Sakamoto, and S. Tanaka, Nucl. Phys. **A174**, 539 (1971).
[23]J. D. King and C. W. Cheng, Can. J. Phys. **57**, 286 (1979); **57**, 1063(E) (1979).
[24]M. Paul, W. Henning, W. Kutschera, E. J. Stephenson, and J. L. Yntema, Phys. Lett. **94B**, 303 (1980).
[25]E. B. Norman, K. T. Lesko, T. E. Chupp, and P. Schwalbach, Nucl. Phys. **A357**, 228 (1981).
[26]E. B. Norman, T. E. Chupp, K. T. Lesko, P. Schwalbach, and P. J. Grant, Astrophys. J **251**, 834 (1981).
[27]E. B. Norman, T. E. Chupp, K. T. Lesko, P. Schwalbach, and P. J. Grant, Nucl. Phys. **A390**, 561 (1982).
[28]R. T. Skelton, Ph.D. thesis, California Institute of Technology, 1985.
[29]W. A. Fowler, G. R. Caughlan, and B. A. Zimmerman, Annu. Rev. Astron. Astrophys. **5**, 525 (1967).
[30]F. M. Mann, Hanford Engineering and Development Labora-

tory Report No. HEDL-TME 78 83, 1983 (unpublished); see also J. Thomas, M. R. Zirnbauer, and K. Langanke, Phys. Rev. C **33**, 2197 (1986).

[31]G. R. Caughlan, W. A. Fowler, M. J. Harris, and B. A. Zimmerman, At. Data Nucl. Data Tables **32**, 197 (1985).

[32]N. Prantzos and M. Cassé, Astrophys. J. **307**, 324 (1986).

[33]A. E. Champagne, A. B. McDonald, T. F. Wang, A. J. Howard, P. V. Magnus, and P. D. Parker, Nucl. Phys. **A451**, 498 (1986).

[34]P. Schmalbrock. T. R. Donoghue, M. Wiescher, V. Wijekumar, C. P. Browne, A. A. Rollefson, C. Rolfs, and A. Vlieks, Nucl. Phys. **A457**, 182 (1986).

[35]L. Buchmann, M. Hilgemeier, A. Krauss, A. Redder, C. Rolfs, and H. P. Trautvetter, Nucl. Phys. **A415**, 93 (1984).

[36]H. P. Trautvetter, H. W. Becker, U. Heineman, L. Buchmann, C. Rolfs, F. Käppeler, M. Baumann, H. Freiesleben, H.-J. Lütke-Stetzkamp, P. Geltenbort, and F. Gönnenwein, Z. Phys. A **323**, 1 (1986).

[37]M. J. Harris, W. A. Fowler, G. R. Caughlan, and B. A. Zimmerman, Annu. Rev. Astron. Astrophys. **21**, 165 (1983).